

PAPER

Edge Raman enhancement at layered PbI_2 platelets induced by laser waveguide effect

To cite this article: Heyi Ma *et al* 2022 *Nanotechnology* **33** 035203

View the [article online](#) for updates and enhancements.

You may also like

- [Influence of \$\text{TiO}_2\$ and Si on the exciton–phonon interaction in \$\text{PbI}_2\$ and CdS semiconductors evidenced by Raman spectroscopy](#)
A Nila, I Baltog, D Dragoman *et al.*
- [Enhanced Raman scattering of graphene by silver nanoparticles with different densities and locations](#)
Hai-Bin Sun, Can Fu, Yan-Jie Xia *et al.*
- [Temperature dependence of Raman enhancement induced by Au nanorods array](#)
Yanru Xu, Yanqing Wang, Yixin Chen *et al.*






EDINBURGH INSTRUMENTS

WORLD LEADING MOLECULAR SPECTROSCOPY SOLUTIONS

edinst.com

The advertisement features a red background with the Edinburgh Instruments logo on the left, which consists of a circular pattern of white dots. In the center, there are several pieces of laboratory equipment, including a spectrometer labeled 'FSS' and another labeled 'FLS 1000'. The text 'WORLD LEADING MOLECULAR SPECTROSCOPY SOLUTIONS' is written in white, bold, uppercase letters. The website 'edinst.com' is displayed in a white box in the bottom right corner.

Edge Raman enhancement at layered PbI_2 platelets induced by laser waveguide effect

Heyi Ma^{1,2,7}, Xianxin Wu^{2,3,7}, Wenna Du^{2,3,4,*} , Liyun Zhao⁵,
Yangguang Zhong², Shulin Chen⁶, Peng Gao⁶, Shuai Yue^{2,3},
Qing Zhang⁵ , Wei Liu^{1,*} and Xinfeng Liu^{2,3,*} 

¹ School of Chemical Sciences, University of Chinese Academy of Sciences, Beijing 100049, People's Republic of China

² CAS Key Laboratory of Standardization and Measurement for Nanotechnology, CAS Center for Excellence in Nanoscience, National Center for Nanoscience and Technology, Beijing 100190, People's Republic of China

³ University of Chinese Academy of Sciences, Beijing 100049, People's Republic of China

⁴ Key Laboratory of Semiconductor Materials Science, Beijing Key Laboratory of Low Dimensional Semiconductor Materials and Devices, Institute of Semiconductors, Chinese Academy of Sciences, Beijing 100083, People's Republic of China

⁵ School of Materials Science and Engineering, Peking University, Beijing 100871, People's Republic of China

⁶ Electron Microscopy Laboratory, International Center for Quantum Materials, School of Physics, Peking University, Beijing 100871, People's Republic of China

E-mail: duwn@nanoctr.cn, weiliu@ucas.ac.cn and liuxf@nanoctr.cn

Received 13 April 2021, revised 6 September 2021

Accepted for publication 9 October 2021

Published 29 October 2021



Abstract

As a two-dimensional (2D) layered semiconductor, lead iodide (PbI_2) has been widely used in optoelectronics owing to its unique crystal structure and distinctive optical and electrical properties. A comprehensive understanding of its optical performance is essential for further application and progress. Here, we synthesized regularly shaped PbI_2 platelets using the chemical vapor deposition method. Raman scattering spectroscopy of PbI_2 platelets was predominantly enhanced when the laser radiated at the edge according to Raman mapping spectroscopy. Combining the outcome of polarized Raman scattering spectroscopy and finite-difference time domain simulation analysis, the Raman enhancement was proven to be the consequence of the enhancement effects inherent to the high refractive index contrast waveguide, which is naturally formed in well-defined PbI_2 platelets. Because of the enlarged excited area determined by the increased propagation length of the laser in the PbI_2 platelet formed waveguide, the total Raman enhancements are acquired rather than a localized point enhancement. Finally, the Raman enhancement factor is directly related to the thickness of the PbI_2 platelet, which further confirms the waveguide-enhanced edge Raman. Our investigation of the optical properties of PbI_2 platelets offers reference for potential 2D layered-related optoelectronic applications.

Supplementary material for this article is available [online](#)

Keywords: PbI_2 platelets, layered materials, edge raman enhancement, waveguide effect

(Some figures may appear in colour only in the online journal)

⁷ These authors contributed equally to this work.

* Authors to whom any correspondence should be addressed.

Introduction

Lead iodide (PbI_2) has been demonstrated as a promising material system for fundamental research and technological applications owing to its unique properties, such as a layered structure, non-dangling bond surfaces, thickness-dependent energy band structures, and strong exciton-phonon interactions [1–5]. PbI_2 consists of basic repeating elements as three hexagonally close-packed layers with iodide ions in the top and bottom layers and lead ions in the middle layer, which denotes it as a layered material [6]. Different layers are connected by van der Waals interactions. This layered 2D semiconductor material has a characteristic atomic thickness, and plays an important role in ultrathin and stretchable optoelectronics [1, 7]. This sandwich structure causes charge carrier dynamics perpendicular to these planes exhibit several quantum characteristics that differ significantly from those of traditional 2D layered semiconductors [8–15]. It has been widely employed in the fields of photoelectric, optical detectors, sensors and photocatalysis [11, 16–18].

Another significant feature of 2D layered PbI_2 is its thickness-dependent optoelectronic properties. It has been reported in theory that the energy band structure of layered PbI_2 can shift from a direct band gap to an indirect band gap by changing the layer thickness [19], which can lead to variable optoelectronic properties. This tunable property makes PbI_2 widely used in flexible optoelectronic devices [20, 21]. Additionally, because there are no surface dangling bonds, a layered PbI_2 laser can maintain good device performance for a long time even in a few atomic layers [22]. A solid planar laser using PbI_2 as a gain medium can be easily integrated into a heterogeneous substrate, presenting broad prospects for making chip-level light sources [23–25]. Moreover, PbI_2 is a precursor in the synthesis of organic-inorganic hybrid and fully inorganic lead halide perovskites [26–31], which has attracted wide attention in the fields of photovoltaic and low-threshold lasers in recent years [22, 32–34]. Research on PbI_2 could contribute to further understand the photophysical properties of perovskite solar cells [35–37] and lasers.

Raman spectroscopy plays an important role in exploring the components and structures of substances in the fields of materials, physics, chemistry and biology [38–44]. In this work, 2H- PbI_2 platelets were synthesized on mica substrates via the chemical vapor deposition (CVD) method. Raman enhancement was observed when the laser was irradiated at the edge of the PbI_2 platelet. Supposedly, this phenomenon results from a waveguide effect where laser confines inside and multiple total reflections because of the high refractive contrast between PbI_2 and the surroundings. Compared to the condition when the laser irradiated the center of the PbI_2 platelet, the formed waveguide promoted an increase in the excited area of the laser in the PbI_2 platelet, thus achieving the total enhanced Raman intensity. We further verified the mechanism of waveguide Raman enhancement using polarized Raman measurement, finite-difference time domain (FDTD) simulation and relationship characterization between the Raman enhancement factor and sample thickness.

Results and discussions

Figure 1(a) shows an optical image of PbI_2 platelets grown using the CVD method. The PbI_2 platelet has a well-defined triangular shape with different colors indicating different thicknesses, which was confirmed by atomic force microscope (AFM) characterization, as shown in figure 1(b). The enlarged scanning electron microscope (SEM) image of the PbI_2 platelet exhibits smooth surface with neat edges (figure 1(c)) implying the high quality of these PbI_2 platelets. High-resolution transmission electron microscopy (HRTEM) and selected-area electron diffraction (SAED) images of the PbI_2 platelets were further conducted to study the crystal structure (figures 1(d) and (e)). The HRTEM image is viewed along the [001] zone axis and the crystal can be described as single crystals along [001] growth direction. The lattice fringes are clearly observed and the values of 0.23 and 0.39 nm corresponds to d-spacings of the (110) and (100) planes of the hexagonal PbI_2 . The SAED pattern shown in figure 1(e) displays a bright diffraction spot and the hexagonal symmetry, in agreement with the hexagonal atom arrangement of PbI_2 . Our TEM results are consistent with those reported in the literature [21, 22, 45–48]. Figure 1(f) shows the x-ray diffraction (XRD) pattern of PbI_2 platelets. By comparing the peak positions with the standard PDF card (JCPDS: No. 07-0235) shown in the lower panel, the XRD pattern shows only (001) diffraction peaks which is in good agreement with literatures reported [21, 45, 48–52]. It can be concluded that the PbI_2 platelets show a 2H type PbI_2 crystal structure and prefer to have their (001) planes up [53]. All the characterizations demonstrate that the 2H- PbI_2 platelets with good quality were successfully acquired by the CVD method.

The Raman spectra of the PbI_2 platelets were measured using a 532 nm laser. As shown in figure 2(a), there are three prominent Raman peaks at 74 cm^{-1} , 94 cm^{-1} , and 106 cm^{-1} , which can be assigned to the E_g , A_{1g} , and A_{2u} modes, respectively [54, 55]. The insets in figure 2(a) are schematic diagrams of the three Raman modes. Among these, the A_g mode is due to the symmetric stretching of two iodine atoms, the E_g mode is correspond to the shearing motion of two iodine layers, the A_{2u} mode is derived from the stretching of two iodine atoms in the same direction and the lead atom vibrates in the opposite direction. The Raman scattering spectra at different positions were obtained to study the homogeneity of the PbI_2 platelets. Surprisingly, we found that the total Raman intensity when the laser located at the edge (P2) of the sample was several times higher than that at the center (P1) (figure 2(b)). Raman mapping results also confirmed this phenomenon (figure 2(c)). The color at the edge of the sample is much more obvious than that at the center, which indicates that the total Raman intensity acquired when the laser illuminated at the edge is much higher than that at the center. Meanwhile, all the Raman intensities for different modes (E_g , A_{1g} , and A_{2u}) are exactly enhanced with excitation at the edge, as shown by the Raman mapping of the individual modes illustrated in figures 2(d)–(f). This experimental phenomenon indicates that this edge Raman enhancement has no specific mode selectivity and little relationship with the phonon energy.

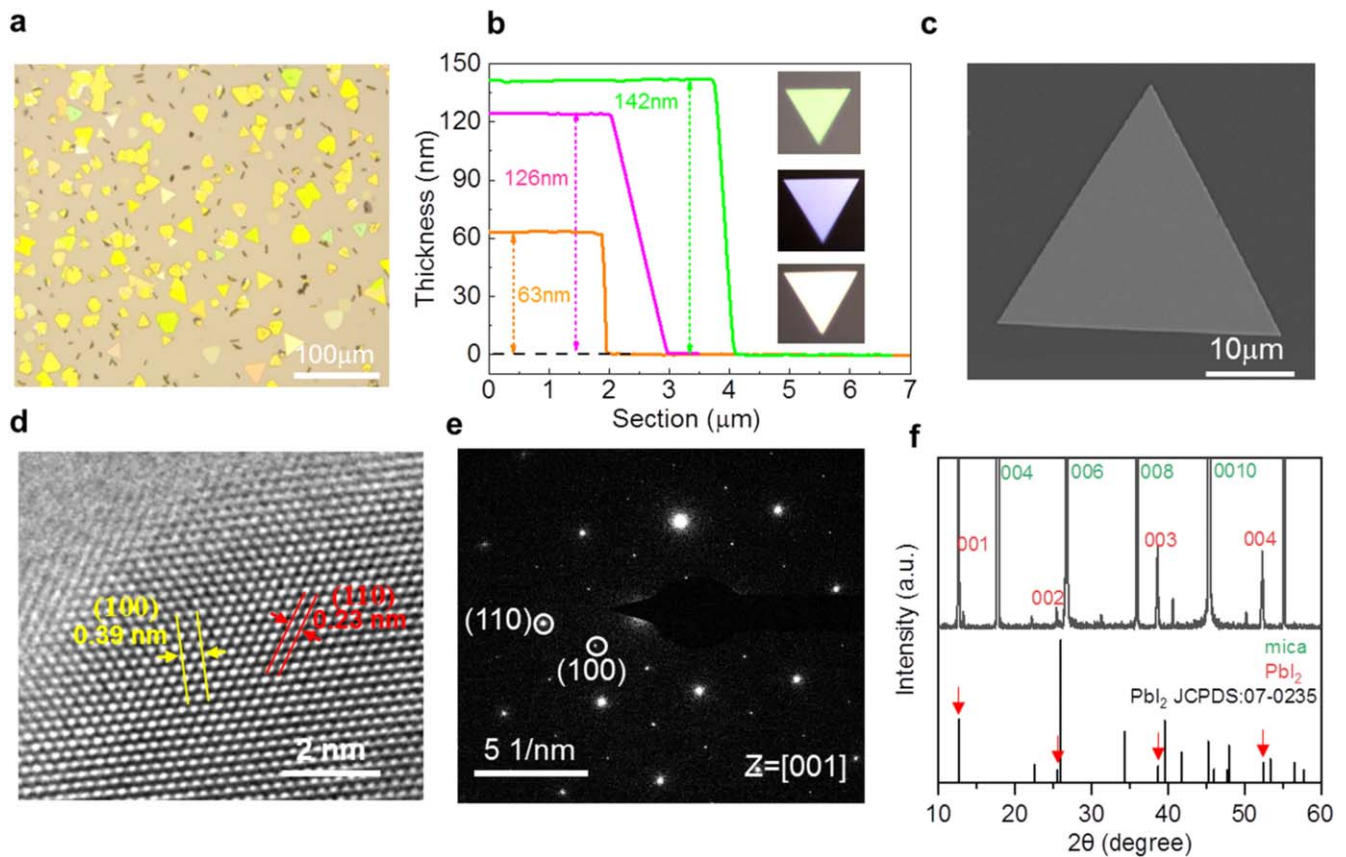


Figure 1. Characterizations of chemical vapor deposited PbI_2 platelets. (a) The optical photograph of as-grown PbI_2 platelets. (b) Three AFM of different thickness PbI_2 platelets. Their thicknesses are 63 nm, 126 nm, 142 nm, respectively. (c) The SEM image of a representative PbI_2 platelet. (d)–(e) The TEM and SAED of PbI_2 platelets show the 2H crystal phase and the distance of (110) and (100). (f) The XRD of as-grown PbI_2 platelets. The green labelled peaks represent mica, and the red peaks are from PbI_2 platelets. The standard data file (PDF No. 7-235) are compared in the lower panel and the red arrow indicates the (00l) diffraction peaks.

The edge Raman enhancement effect of PbI_2 platelets is mainly explained by three mechanisms, according to previous literatures [56–59]. The first hypothesis is that the enhancement effect in PbI_2 platelets is related to the non-uniform distribution of the iodine and lead content in the samples or the edge defects. By measuring the energy dispersive x-ray spectroscopy (EDX) of PbI_2 platelets (figure S1(a) (available online at stacks.iop.org/NANO/33/035203/mmedia)), the results show that the iodide and lead content at the edge of the sample were the same as those at the center. Additionally, the absorption spectra at the edge show no additional defect-related peaks and almost the same line shape as that at the center (figure S1(b)) [17]. The results indicate that the type and distribution of the elements in the obtained PbI_2 platelet samples at the edge are the same as those at the center. Meanwhile, there were no defects and no change in the band structure at the edge. Therefore, we speculate that the edge Raman enhancement was not caused by the element content difference or edge defect states.

The second hypothesis is that the Raman enhancement at the edge of the PbI_2 platelet is related to the resonance between the incident laser and the wave modes of the PbI_2 exciton [57]. For this case, we explored the temperature-dependence fluorescence and Raman measurements of PbI_2 platelets as shown in figures S2 and S3. As seen from the

temperature-dependence photoluminescence (PL) spectrum as the temperature decreased from 280 to 80 K, the PL peak position of PbI_2 platelets exhibits a significant blue shift from 508.8 to 497.2 nm, accompanied by a significant increase in the peak intensity. If the edge Raman enhancement effect is related to the resonance of the incident laser and PbI_2 platelets exciton mode, the shift of the PL peak position and the consequent displacement with respect to the incident laser wavelength position will affect the resonance effects. The edge Raman enhancement factor should also be expected to exhibit temperature-dependence. However, the Raman intensity (figure S3) showed no significant change with temperature at the edge and center of the PbI_2 platelet; that is, the Raman enhancement was independent of the resonance between the incident laser wavelength and the exciton peak position of PbI_2 platelets.

The third hypothesis is that the Raman enhancement resulted from the waveguide-enhanced Raman spectra (WERS). The WERS could enhanced the Raman signal using the optical waveguide produced on the surface of the materials and several efforts have been made to understand the WERS [58, 60]. Because of the high index contrast between the structure and substrate, as well as the structure and air, light get totally reflected at the interfaces above critical angle of incidence. Then light rays bounce back and forth between

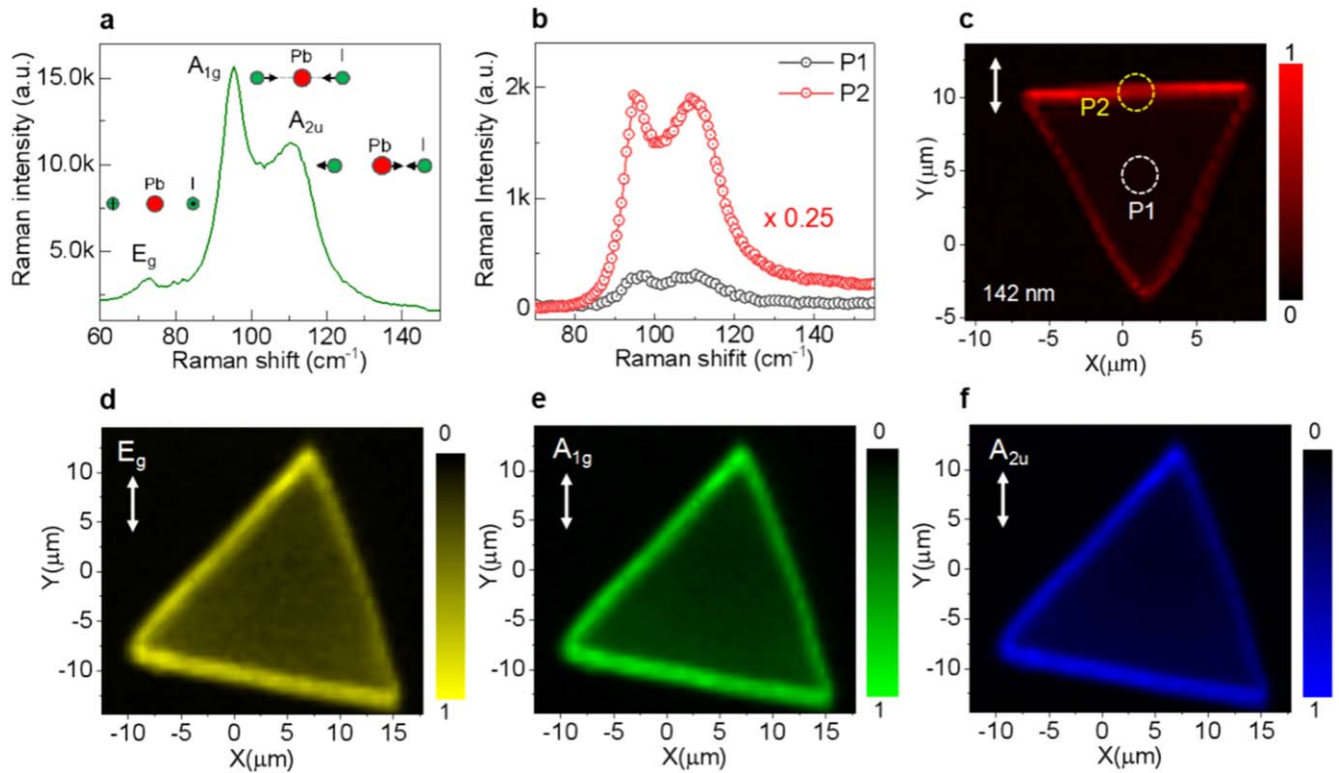


Figure 2. (a) The single representative Raman spectra of PbI₂ platelets. There are three Raman modes which are the E_g, A_{1g} and A_{2u}. Their position of Raman modes is at 74 cm⁻¹, 94 cm⁻¹, and 106 cm⁻¹. (b) Raman spectrum of the edge (P2) and center (P1) of the PbI₂ platelets observed by polarized laser perpendicular to the upper edge corresponding to the positions labeled in (c). (c) The Raman mapping of the PbI₂ platelets. (d)–(f) The Raman mapping of the E_g, A_{1g} and A_{2u} modes. These arrows indicate the polarized direction of the incident laser.

the two interfaces, and travel in the structure, forming a waveguide. The magnitude of the Raman excitation, determined by the interface intensity and number of excited molecules, is closely related to the waveguide dimension. Guided light reflected back and forth in the waveguide leads to an equivalent of approximately 10^3 – 10^6 reflections cm⁻¹, depending upon which waveguide mode the light travels in. Compared to the conventional Raman spectroscopy configuration, where light is incident and reflected only once, these multiple reflections essentially contribute to the large intensity on the waveguide surface (interface). Light confined into a small dimension by the waveguide structure not only gets effectively ‘focussed’, which leads to a similar level of high intensity, but also maintains this high intensity over a much longer range (10^3 – 10^4 more by assuming low loss propagation in a few centimeters), which is proportional to the number of excited molecules for a surface uniformly covered with analyte. Therefore, high intensity and large sampling area in WERS boost the Raman scattered power on the waveguide surface, which are the main reasons for the ‘enhancement’ in WERS. Figure 3(a) shows a schematic of the waveguide Raman enhancement. First, a laser beam vertically strikes the plane of PbI₂ platelets, with the incident point at the edge, and the laser polarization is perpendicular to the edge in the plane of PbI₂ platelets. Because of the high refractive index contrast between the PbI₂ platelets and mica substrate as well as the PbI₂ platelets and air, the incident laser couples into the PbI₂ platelet and are totally reflected at

the interfaces, forming a waveguide in the platelet. It propagates along the direction of the coupled laser polarization, and the laser bounces back and forth between the top and bottom surfaces of the PbI₂ platelets, indicating a large sampling area that essentially contributes to the large intensity on the whole waveguide. Moreover, light confined into a small dimension by the waveguide is effectively ‘focussed’, producing a corresponding non-uniform electric field with high intensity along the waveguide. The waveguide first transforms from the first edge to the second edge, and then the waveguide reflects towards the third edge owing to the angle of incidence between the waveguide and the second edge being relatively large.

Subsequently, because the wave-guiding laser is nearly perpendicular to the third edge, it finally leaks out. During the entire process, high intensity and large sampling area in the WERS boost the Raman scattered power on the waveguide. In contrast, when laser beam strikes the center of the PbI₂ platelets, the laser cannot be effectively coupled into the platelets and thus cannot propagate by continuous reflection between the upper and lower surfaces of the PbI₂ platelets to form the waveguide.

This phenomenon can be confirmed using the light distribution in the dark field optical images of figures 3(b) and (c). Figure 3(b) shows the optical image of laser irradiation in the center of PbI₂ platelets. It is noted that there are no signals of laser leakage from the three edges, demonstrating no waveguide formation and no propagation of the laser. Figure 3(c) presents

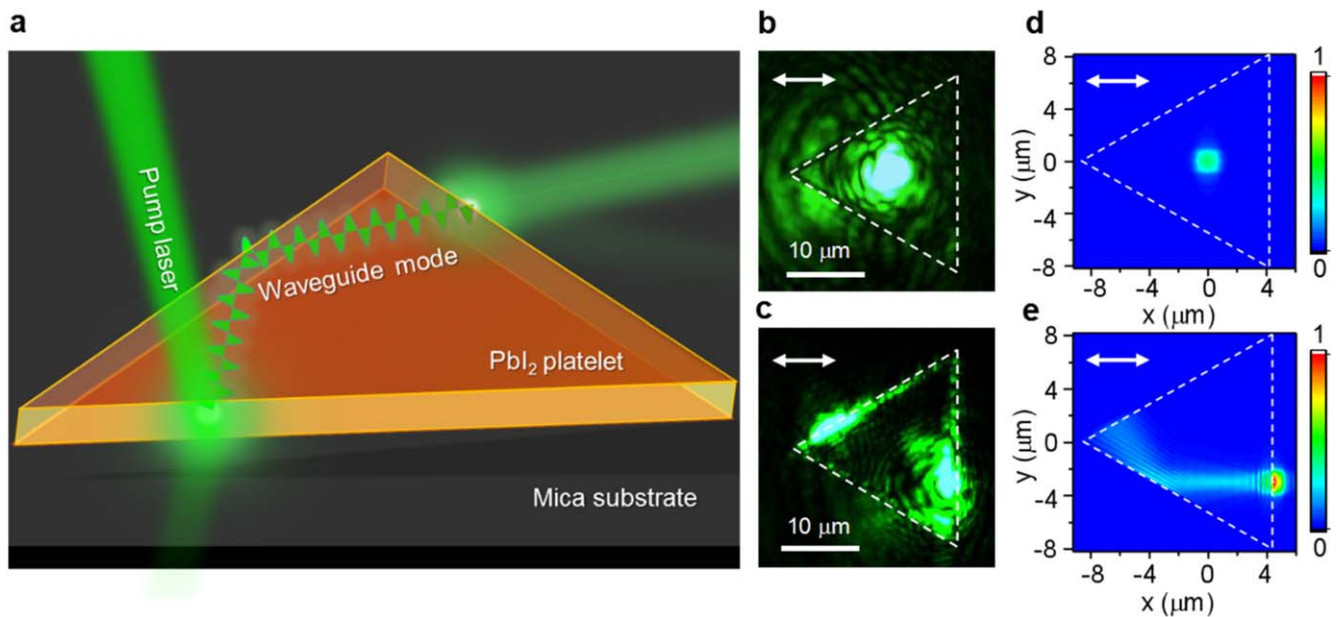


Figure 3. (a) Schematic diagram of the waveguide generate, and laser spread inside the PbI_2 platelets and leak out from one edge. The dark field optical image of PbI_2 platelets, where laser incident is located at the center (b) and edge (c). (d), (e) The simulation of the electric field distribution of PbI_2 platelets by FDTD, which laser incident at the (d) center and (e) edge. The polarization of the excitation beam is shown in the form of arrow.

an image of laser irradiation at the edge of the PbI_2 platelet. The laser was clearly observed leaking from the other edge. This mechanism was further validated by simulating the FDTD method. Figures 3(d) and (e) show the electric field distributions of laser irradiation at the center and edge of the PbI_2 platelet. When the laser strikes the center of the sample, there is no enhancement in the electric field signal laser propagation (figure 3(d)). However, when the laser strikes the edge of the PbI_2 platelets, an electric field inside the sample intensifies and propagates along the direction of the laser polarization (figure 3(e)). Hence, our simulated results of the electric field distribution are consistent with the conjecture and experimental phenomena of the optical image.

Figure 4(a) shows a schematic of the polarized Raman scattering experiment. The laser was irradiated vertically on the edge of the sample, and the angle between the laser polarization direction and the edge of θ was tuned by rotating the sample. When the sample was rotated, the polarization angle of the incident laser changed synchronously. The polarization change has little effect on the Raman intensity at the center (figure 4(c)) while it leads to almost four-fold difference in the Raman intensity at the edge of the sample with different polarization directions (figure 4(d)). As shown in figure 4(b) extracted from figures 4(c) and (d), the angle dependence of the A_{1g} mode Raman intensity for the laser irradiated at the edge exhibits two-fold symmetry (Raman intensity of A_{2u} mode has similar behavior plotted in figure S4). When the polarization of the incident laser is parallel to the edge of the PbI_2 platelets (i.e. $\theta = 0^\circ$ or 180°), the Raman intensity is the lowest. When the polarization of the incident laser is perpendicular to the edge of the PbI_2 platelets (i.e. $\theta = 90^\circ$ or 270°), the Raman intensity reaches its maximum value. When the incident laser beam strikes at the center of the sample, the change in polarization

does not lead to a distinct change in the Raman intensity. When the laser is irradiated at the center of the sample, the laser will not couple to the PbI_2 platelet, so the Raman intensity does not change with the laser polarization angle. However, when the laser is irradiated on the edge of the sample, the components perpendicular to the edge of the sample are different for different polarization angles, and the proportion of laser coupled into the PbI_2 platelet is different. This can result in different Raman enhancement factors. Therefore, at this point, edge Raman enhancement is related to the angle of polarization. This law is consistent with that shown in the optical image with different laser polarization angles irradiated at the sample (figure S5). From figure S5, when the laser is irradiated at the edge of the PbI_2 platelets and the polarization direction of the laser is perpendicular to the edge of the sample, the laser intensity emitted from the other edge is the highest, which indicates the largest amount of coupled laser flux. When the laser polarization direction is parallel to the edge of the sample, the laser intensity emitted from the other side is the lowest, which indicates the least amount of coupled laser flux. Because the incident point of the laser is the same, the propagation path of laser coupling into the sample is identical regardless of how the θ changes, that is, the interaction area of the laser and PbI_2 platelet is the same. Therefore, the more the laser intensity coupled in, the larger the Raman enhancement factor of the edge. In other words, when the polarization angle of the laser is perpendicular to the edge of the sample, most of the laser flux is coupled into the sample, and the enhancement factor is the largest. When the laser hits the center of the sample, the Raman intensity does not vary with the polarization angle of the laser. The results should match the schematic diagram of the Raman enhancement principle (figure 3(a)) and the electric field simulation diagram of PbI_2 platelets (see figures 3(c) and (e)). Therefore, we speculate that

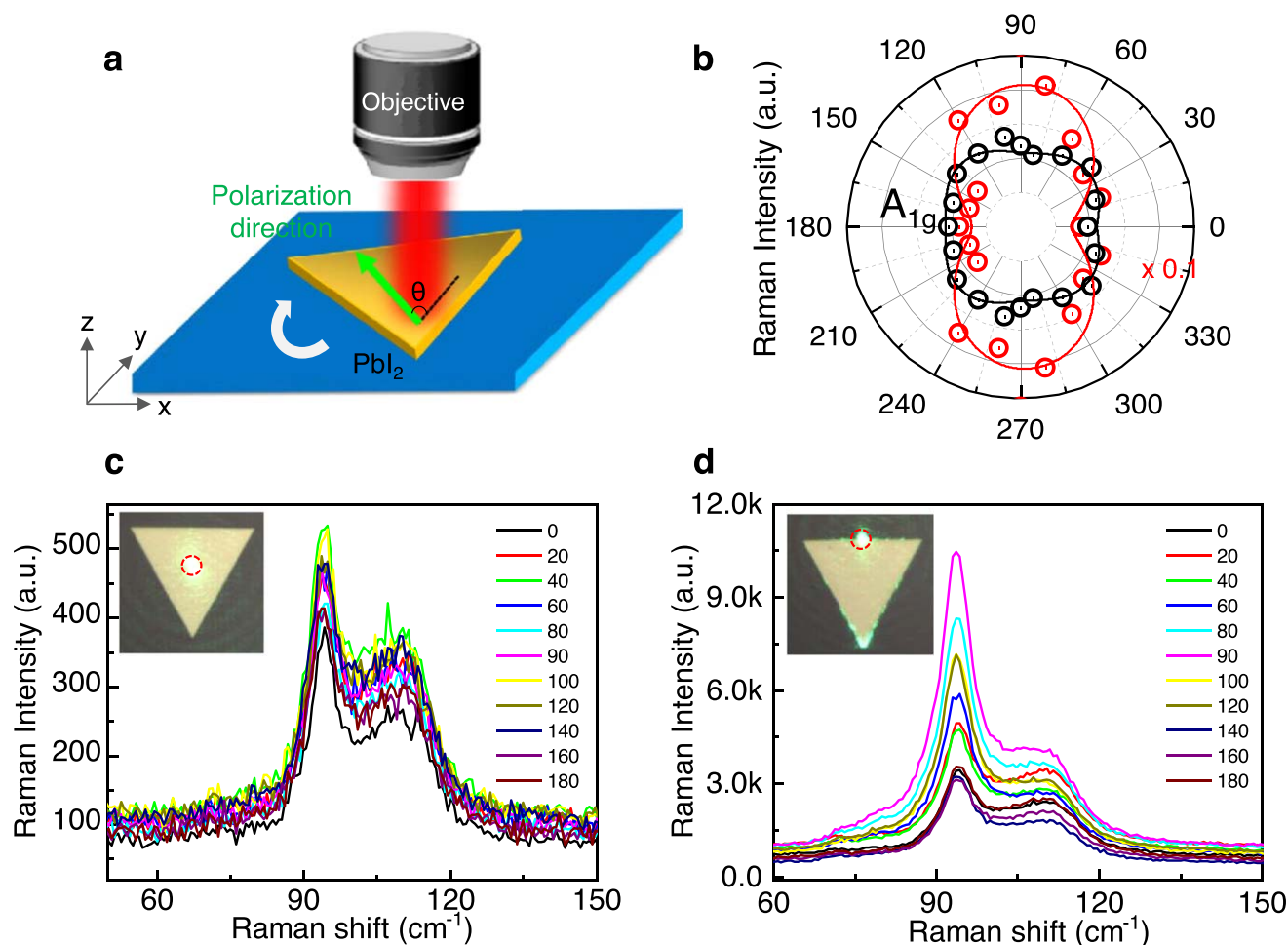


Figure 4. (a) The schematic diagram of the polarized Raman scattering experiment. (b) The Raman intensity distribution for A_{1g} mode of different angles between the laser polarization direction and the edge for laser exciting at edge (red) and center (black). The Raman intensity at the edge is related to the polarization angle of the laser. To the contrary, the Raman intensity at the center has no contact with the polarization angle of the laser. (c)–(d) Raman spectrum of different laser polarization angle on PbI_2 platelets at the center (c) and edge (d).

the Raman intensity of the edge of PbI_2 is related to the laser intensity emitted from the edge of the sample, the higher the laser intensity emitted from the edge, the higher the Raman intensity. From another perspective, it was verified that the edge Raman enhancement effect of the PbI_2 platelets is caused by the waveguide. Additionally, as shown in figure 4(d) the enhancement multiples for the A_{1g} and A_{2u} modes under different polarization conditions are different. Our analysis (figure S6) revealed that the enhancement factor of the A_{1g} mode is slightly larger than that of the A_{2u} mode, especially for θ close to 90° . This may suggest that the Raman enhancement is not only related to the difference in the coupling laser flux, but also to the polarization direction of the excitation laser. The underlying reason for this is still unclear and further studies are needed.

Subsequently, the influence of the thickness on the enhancement factor was investigated using experiment and simulation. We measured the Raman intensity when laser exposed to the edge and center of the PbI_2 platelets under different thicknesses, as determined by AFM. From the Raman mapping of PbI_2 platelets with different thicknesses (figure S7), it is that the edge Raman signal can be enhanced in samples with

a large-spanded thickness, and the edges of the triangular PbI_2 platelet become clearer with a larger thickness. The Raman spectra of different thickness PbI_2 platelets of different thicknesses at center and edges are shown in figure S8. We can obtain a scaling law for the Raman enhancement factor (the ratio of Raman intensity between the edge and the center of PbI_2 platelets) with the thickness of the sample as the green solid dots plotted in figure 5(a). In our experiment, when the thickness was smaller than the value (~ 150 nm), the edge Raman enhancement factor increases monotonically with an increase in the sample thickness. We suppose that the greater the sample thickness, the larger the interaction area between PbI_2 platelets and the laser, which leads to a greater Raman enhancement factor. The Raman enhancement factor decreased slightly for a thickness of ~ 200 nm. Additionally, little Raman shift can be seen from the thickness-dependent spectra (figure S8), indicating that the 2D platelets we synthesized are insensitive to strains or charge transfer doping across the interfaces (see Supporting Information, VIII).

To gain a deeper understanding of the Raman enhancement achieved in PbI_2 platelets, FDTD numerical simulations

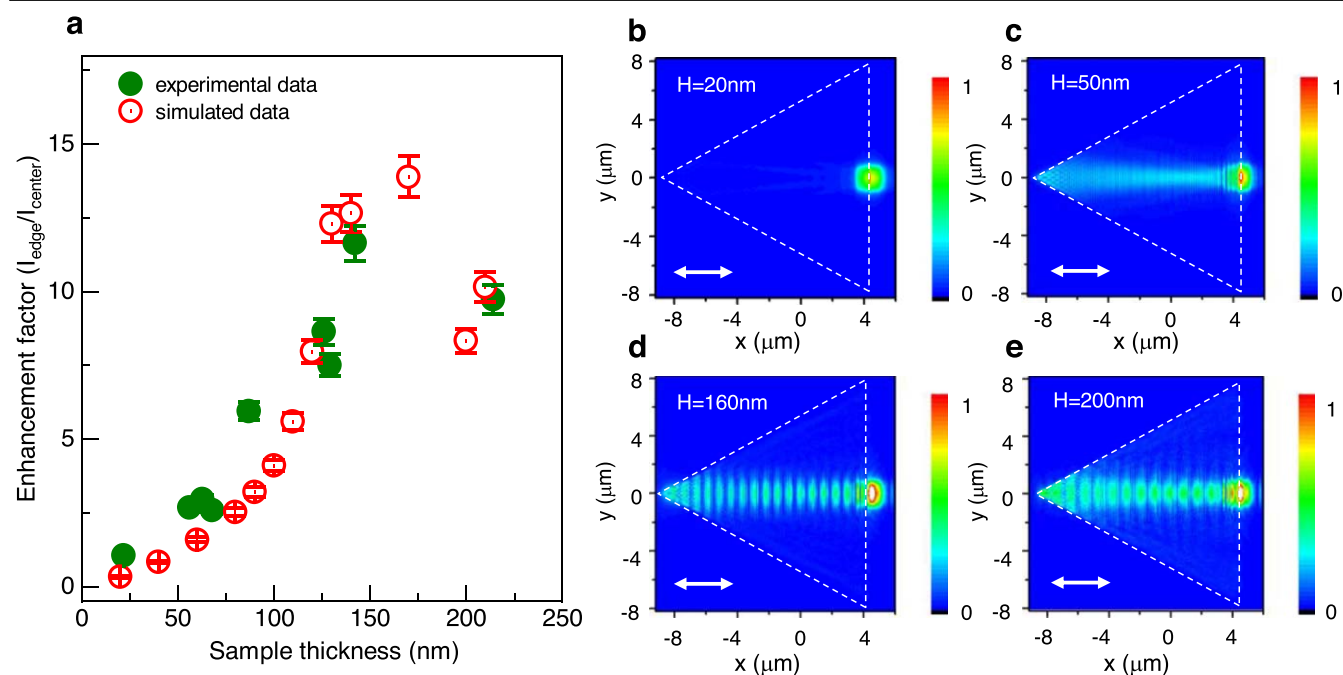


Figure 5. (a) The relationship between the thickness and enhancement factor, which is the ratio of Raman intensity between the edge and the center of PbI_2 platelets. The experimental data are solid green dots, simulation data are red hollow dots. There is a good match between the experimental and the simulation data. (b)–(e) The simulation of the electric field distribution of PbI_2 platelets with different thicknesses, where the incident laser locates at the edge. The larger thickness of the PbI_2 platelet is, the higher the edge Raman enhancement factor produced.

were conducted. Using FDTD simulation, we obtained the laser field distribution of PbI_2 platelets with different thicknesses (figures 5(b)–(e) and S9). When the laser strikes the center of the sample, there is no laser propagation for all thickness samples and the electric field intensity fluctuates slightly. The corresponding total electric field intensities are plotted in figure S10. Note that the electric field intensity oscillates periodically with thickness of the laser hitting the center. The maximum value of the electric field occurs at an integer multiple of ~ 100 nm in thickness. Considering the incident wavelength $\lambda \approx 532$ nm and the refractive index $n \approx 2.56$, from our experimental results, the period thickness matches the function, $d = m\lambda/2n$, where m is an integer. Therefore, we attribute this periodic oscillation phenomenon to the formation of a vertical F-P cavity with the top and bottom surfaces serving as two reflectors. The maximum energy confinement occurs when the thickness of the PbI_2 platelet satisfies the expression of $m\lambda/2n$, representing the occurrence of the maximum confinement factor [61]. However, when the laser strikes the edge of the sample, laser propagation can be clearly observed, and the total electric field intensity increases progressively with increasing thickness. Then the simulated Raman enhancement factor (the ratio of electric field squared) with various thicknesses was also drawn as a red hollow dot in figure 5(a). The correlation between the simulated and experimental results is high, which confirms the mechanism of WERS in our system. Meanwhile, the decrease in the Raman enhancement factor at a thickness of ~ 200 nm could also be ascribed to the periodic maximum of the electric field for laser striking on the platelet center.

Conclusions

In conclusion, we have reported PbI_2 platelets fabricated by CVD. The morphology and structure characterization results demonstrated that the as-prepared 2H- PbI_2 platelets exhibited high crystallinity. Raman mapping measurements revealed that the total Raman intensity when the laser struck at the edge of the PbI_2 sample was several times higher than when the laser radiated at the center. The Raman enhancement effect was ascribed to WERS from the high refractive index contrast and the subsequent formation of the waveguide. The high intensity of laser in a longer range and large sampling area in the WERS boost the Raman scattered power on the whole waveguide. Our proposed mechanism can also be supported by polarized Raman measurements and simulation results obtained using FDTD method, and the calculated Raman enhancement factors were in good agreement with the experimental data. Finally, WERS can explain the existences of a monotonically increasing relationship between the thickness of PbI_2 and the edge enhancement factor. These results will not only advance the fundamental understanding of the Raman enhancement effect in 2H- PbI_2 , but will also provide an ideal material system for optoelectronic applications.

Experimental section

PbI₂ platelet synthesis and characterization

PbI_2 powder (Aldrich, 99.999%) was used as the reaction precursor and placed in the center of a single-zone furnace

quartz tube (Lindberg Blue M TF55035C-1). A freshly cleaved muscovite mica substrate ($2 \times 4 \text{ cm}^2$) was placed in the downstream region of the quartz tube. The quartz tube was then evacuated to a base pressure of 5×10^{-3} Torr followed by a 30 sccm flow of high-purity argon gas. The temperature was then heated to $380 \text{ }^\circ\text{C}$ for 38 min. The growth pressure was 250 Torr, and the growth time was 20 min. The SEM images and the phase compositions of the PbI_2 platelets were examined through energy dispersive x-ray spectroscopy (EDX) by SEM (Hitachi, S4800). The HRTEM images and SAED patterns of PbI_2 platelets were obtained using a Tecnai F20 instrument. The crystallographic structures of PbI_2 platelets were acquired using (XRD, SmartLab) equipment. The surface morphology and thickness of the PbI_2 platelets were characterized using AFM (dimension icon).

Absorption

The white light as the light source was first irradiated in the silver mirror and reflected back to the spectrograph using the objective lens of the microscope. The detected light intensity was recorded as a . Then, the white light was irradiated in the PbI_2 platelets. A part of the white light was absorbed and the rest was reflected in the spectrograph. Similarly, the obtained light intensity was denoted as b . Thus, the absorptivity of light was calculated using the formula, $\alpha = (a - b)/a$. Given the fact that the fabricated PbI_2 platelet is a direct band gap semiconductor, the absorption spectrum can be obtained with $(\alpha h\nu)^2$ as the Y -axis and $h\nu$ as the X -axis. The forbidden bandwidth is obtained from the absorption spectrum.

Raman spectroscopy

For the Raman spectra experiment, SmartRaman confocal-micro-Raman module was used, which was developed by Institute of Semiconductors, Chinese Academy of Sciences. A 532 nm solid state laser was focused onto the samples using a $100\times$ objective lens, in a non-confocal optical path. The Raman signal was collected using the same objective lens and analyzed using a monochromator equipped with a charge coupled device (CCD) detector.

Temperature-dependent PL spectroscopy

For the PL spectra experiment, we placed the sample in a cryogenic chamber and vacuum it. Liquid nitrogen was used to decrease the temperature. A 405 nm continuous wave laser was focused onto the samples by a $50\times$ objective lens. The PL signal was collected using the same objective lens and analyzed using a monochromator equipped with a CCD detector. The fluorescence spectra of the PbI_2 platelets were measured at different temperatures.

Simulations

FDTD simulations were performed using Lumerical (a commercial software). The model of the PbI_2 triangular micro-plate was built according to the experimental geometry, which was placed on a mica substrate block with a side length of $15 \mu\text{m}$ and

thickness ranging from 20 to 230 nm (figure S10). A Gauss beam ($r = 1 \mu\text{m}$) of 532 nm was used to excite the micro-plate from both the edge and center of the triangular micro-plate. The permittivity of the materials was calculated from the expression for the high-frequency refractive index [62].



Acknowledgments

HM and XW contributed equally to this work. The authors thank the support of the Ministry of Science and Technology (2017YFA0205004, 2017YFA0205700 and 2017YFA0304600), the Strategic Priority Research Program of Chinese Academy of Sciences (XDB36000000), National Natural Science Foundation of China (22073022, 11874130, 12074086, 22077121, 52072006, 51991340, 51991344 and 22173025), DNL Cooperation Fund, CAS (DNL202016), and Open Research Fund Program of the State Key Laboratory of Low-Dimensional Quantum physics (KF201907). They also acknowledge the Electron Microscopy Laboratory at Peking University for the use of electron microscopes.

Data availability statement

All data that support the findings of this study are included within the article (and any supplementary files).

ORCID iDs

Wenna Du  <https://orcid.org/0000-0003-0023-0183>
Qing Zhang  <https://orcid.org/0000-0002-6869-0381>
Xinfeng Liu  <https://orcid.org/0000-0002-7662-7171>

References

- [1] Radisavljevic B, Radenovic A, Brivio J, Giacometti V and Kis A 2011 Single-layer MoS_2 transistors *Nat. Nanotechnol.* **6** 147–50
- [2] Lopez-Sanchez O, Lembke D, Kayci M, Radenovic A and Kis A 2013 Ultrasensitive photodetectors based on monolayer MoS_2 *Nat. Nanotechnol.* **8** 497–501
- [3] Wu S F *et al* 2013 Electrical tuning of valley magnetic moment through symmetry control in bilayer MoS_2 *Nat. Phys.* **9** 149–53
- [4] Gong Y *et al* 2014 Vertical and in-plane heterostructures from WS_2/MoS_2 monolayers *Nat. Mater.* **13** 1135–42
- [5] Lv R, Robinson J A, Schaak R E, Sun D, Sun Y, Mallouk T E and Terrones M 2015 Transition metal dichalcogenides and beyond: synthesis, properties, and applications of single- and few-layer nanosheets *Acc. Chem. Res.* **48** 56–64
- [6] Beckmann P A 2010 A review of polytypism in lead iodide *Cryst. Res. Technol.* **45** 455–60
- [7] An Y P, Zhang M J, Wu D P, Fu Z M and Wang K 2016 The electronic transport properties of transition-metal dichalcogenide lateral heterojunctions *J. Mater. Chem. C* **4** 10962–6

- [8] Dorner B, Ghosh R E and Harbeke G 1976 Phonon dispersion in the layered compound PbI_2 *physica status solidi b* **73** 655–9
- [9] Watanabe M and Hayashi T 1994 Polariton relaxation and bound exciton formation in PbI_2 studied by excitation-spectra *J. Phys. Soc. Japan* **63** 785–94
- [10] Makino T, Watanabe M, Hayashi T and Ashida M 1998 Time-resolved luminescence of exciton polaritons in PbI_2 *Phys. Rev. B* **57** 3714–7
- [11] Sengupta A, Jiang B, Mandal K C and Zhang J Z 1999 Ultrafast electronic relaxation dynamics in PbI_2 semiconductor colloidal nanoparticles: a femtosecond transient absorption study *J. Phys. Chem. B* **103** 3128–37
- [12] Sun Z P, Martinez A and Wang F 2016 Optical modulators with 2D layered materials *Nat. Photon.* **10** 227–38
- [13] Zhou X, Hu X Z, Zhou S S, Zhang Q, Li H Q and Zhai T Y 2017 Ultrathin 2D GeSe_2 rhombic flakes with high anisotropy realized by van der waals epitaxy *Adv. Funct. Mater.* **27** 1703858
- [14] Yang H, Jussila H, Autere A, Komsa H P, Ye G J, Chen X H, Hasan T and Sun Z P 2017 Optical waveplates based on birefringence of anisotropic two-dimensional layered materials *ACS Photonics* **4** 3023–30
- [15] Autere A, Jussila H, Dai Y, Wang Y, Lipsanen H and Sun Z 2018 Nonlinear optics with 2D layered materials *Adv. Mater.* **30** e1705963
- [16] Goto T and Tanaka H 1994 Exciton study in PbI_2 microcrystallites by pump-probe method *Solid State Commun.* **89** 17–21
- [17] Wang Y G, Gan L, Chen J N, Yang R and Zhai T Y 2017 Achieving highly uniform two-dimensional PbI_2 flakes for photodetectors via space confined physical vapor deposition *Sci. Bull.* **62** 1654–62
- [18] Manjappa M, Solanki A, Kumar A, Sum T C and Singh R 2019 Solution-processed lead iodide for ultrafast all-optical switching of terahertz photonic devices *Adv. Mater.* **31** e1901455
- [19] Frisenda R et al 2017 Characterization of highly crystalline lead iodide nanosheets prepared by room-temperature solution processing *Nanotechnology* **28** 455703
- [20] Zhong M, Huang L, Deng H-X, Wang X, Li B, Wei Z and Li J 2016 Flexible photodetectors based on phase dependent PbI_2 single crystals *J. Mater. Chem. C* **4** 6492–9
- [21] Du L et al 2019 Perseverance of direct bandgap in multilayer 2D PbI_2 under an experimental strain up to 7.69% *2D Mater.* **6** 025014
- [22] Zhong Y et al 2018 Low threshold Fabry–Perot mode lasing from lead iodide trapezoidal nanoplatelets *Small* **14** e1801938
- [23] Liu X, Ha S T, Zhang Q, de la Mata M, Magen C, Arbiol J, Sum T C and Xiong Q 2015 Whispering gallery mode lasing from hexagonal shaped layered lead iodide crystals *ACS Nano* **9** 687–95
- [24] Huang M H, Mao S, Feick H, Yan H, Wu Y, Kind H, Weber E, Russo R and Yang P 2001 Room-temperature ultraviolet nanowire nanolasers *Science* **292** 1897–9
- [25] Blanche P A et al 2010 Holographic three-dimensional telepresence using large-area photorefractive polymer *Nature* **468** 80–3
- [26] Tan Z K et al 2014 Bright light-emitting diodes based on organometal halide perovskite *Nat. Nanotechnol.* **9** 687–92
- [27] Lin Q Q, Armin A, Nagiri R C R, Bum P L and Meredith P 2015 Electro-optics of perovskite solar cells *Nat. Photonics* **9** 106–12
- [28] Li D, Wang G, Cheng H C, Chen C Y, Wu H, Liu Y, Huang Y and Duan X 2016 Size-dependent phase transition in methylammonium lead iodide perovskite microplate crystals *Nat. Commun.* **7** 11330
- [29] Zheng Z, Wang X X, Shen Y W, Luo Z Y, Li L G, Gan L, Ma Y, Li H Q, Pan A L and Zhai T Y 2018 Space-confined synthesis of 2D all-inorganic CsPbI_3 perovskite nanosheets for multiphoton-pumped lasing *Adv. Opt. Mater.* **6** 1800879
- [30] Chen Q et al 2018 All-inorganic perovskite nanocrystal scintillators *Nature* **561** 88–93
- [31] Pang G, Lan X, Li R, He Z and Chen R 2019 Influence of mixed organic cations on the structural and optical properties of lead tri-iodide perovskites *Nanoscale* **11** 5215–21
- [32] Zhang Q, Ha S T, Liu X, Sum T C and Xiong Q 2014 Room-temperature near-infrared high- Q perovskite whispering-gallery planar nanolasers *Nano Lett.* **14** 5995–6001
- [33] Su R, Diederichs C, Wang J, Liew T C H, Zhao J, Liu S, Xu W, Chen Z and Xiong Q 2017 Room-temperature polariton lasing in all-inorganic perovskite nanoplatelets *Nano Lett.* **17** 3982–8
- [34] Du W et al 2018 Strong exciton-photon coupling and lasing behavior in All-Inorganic CsPbBr_3 micro/nanowire fabry-pérot cavity *ACS Photonics* **5** 2051–9
- [35] Kim H S et al 2012 Lead iodide perovskite sensitized all-solid-state submicron thin film mesoscopic solar cell with efficiency exceeding 9% *Sci. Rep.* **2** 591
- [36] Razza S et al 2015 Perovskite solar cells and large area modules (100 cm²) based on an air flow-assisted PbI_2 blade coating deposition process *J. Power Sources* **277** 286–91
- [37] Maitani M M, Tateyama A, Boix P P, Han G F, Nitta A, Ohtani B, Mathews N and Wada Y 2019 Effects of energetics with {001} facet-dominant anatase TiO_2 scaffold on electron transport in $\text{CH}_3\text{NH}_3\text{PbI}_3$ perovskite solar cells *Electrochim. Acta* **300** 445–54
- [38] Wachs I E 1996 Raman and IR studies of surface metal oxide species on oxide supports: supported metal oxide catalysts *Catal. Today* **27** 437–55
- [39] Choi H C, Jung Y M and Kim S B 2005 Size effects in the Raman spectra of TiO_2 nanoparticles *Vib. Spectrosc.* **37** 33–8
- [40] Evans C L, Potma E O, Puoris’haag M, Cote D, Lin C P and Xie X S 2005 Chemical imaging of tissue *in vivo* with video-rate coherent anti-Stokes Raman scattering microscopy *Proc. Natl Acad. Sci. USA* **102** 16807–12
- [41] Movasaghi Z, Rehman S and Rehman I U 2007 Raman spectroscopy of biological tissues *Appl. Spectrosc. Rev.* **42** 493–541
- [42] Liu Z, Davis C, Cai W, He L, Chen X and Dai H 2008 Circulation and long-term fate of functionalized, biocompatible single-walled carbon nanotubes in mice probed by Raman spectroscopy *Proc. Natl Acad. Sci. USA* **105** 1410–5
- [43] Evans C L and Xie X S 2008 Coherent anti-stokes Raman scattering microscopy: chemical imaging for biology and medicine *Annu. Rev. Anal. Chem. (Palo Alto Calif)* **1** 883–909
- [44] Fan M, Andrade G F and Brolo A G 2011 A review on the fabrication of substrates for surface enhanced Raman spectroscopy and their applications in analytical chemistry *Anal. Chim. Acta* **693** 7–25
- [45] Zheng W, Zhang Z, Lin R, Xu K, He J and Huang F 2016 High-crystalline 2D layered PbI_2 with ultrasurface: liquid-phase synthesis and application of high-speed photon detection *Adv. Electron. Mater.* **2** 1600291
- [46] Song H, Karakurt I, Wei M, Liu N, Chu Y, Zhong J and Lin L 2018 Lead iodide nanosheets for piezoelectric energy conversion and strain sensing *Nano Energy* **49** 7–13
- [47] Xiao H, Liang T and Xu M 2019 Growth of ultraflat PbI_2 nanoflakes by solvent evaporation suppression for high-performance UV photodetectors *Small* **15** e1901767
- [48] Zhao J et al 2020 Programmable single-crystalline PbI_2 microplate arrays and their organic/inorganic heterojunctions *Adv. Funct. Mater.* **30** 2003631
- [49] Shkir M, Abbas H, Siddhartha and Khan Z R 2012 Effect of thickness on the structural, optical and electrical properties

- of thermally evaporated PbI₂ thin films *J. Phys. Chem. Solids* **73** 1309–13
- [50] Zhang J, Song T, Zhang Z, Ding K, Huang F and Sun B 2015 Layered ultrathin PbI₂ single crystals for high sensitivity flexible photodetectors *J. Mater. Chem. C* **3** 4402–6
- [51] Zhang J et al 2018 Low-temperature heteroepitaxy of 2D PbI₂/graphene for large-area flexible photodetectors *Adv. Mater.* **30** e1803194
- [52] Lin G, Dai L and Hsu H 2019 PbI₂ Single crystal growth and its optical property study *Crystals* **9** 1600291
- [53] Ha S T, Liu X, Zhang Q, Giovanni D, Sum T C and Xiong Q 2014 Synthesis of organic-inorganic lead halide perovskite nanoplatelets: towards high-performance perovskite solar cells and optoelectronic devices *Adv. Opt. Mater.* **2** 838–44
- [54] Khilji M Y, Sherman W F and Wilkinson G R 1982 Raman study of three polytypes of PbI₂ *J. Raman Spectrosc.* **13** 127–33
- [55] Pedesseau L, Even J, Katan C, Raouafi F, Wei Y, Deleporte E and Jancu J M 2013 vibrational properties of 2H-PbI₂ semiconductors studied via density functional theory calculations *Thin Solid Films* **541** 9–11
- [56] Yano T-A, Yoshida K, Hayamizu Y, Hayashi T, Ohuchi F and Hara M 2015 Probing edge-activated resonant raman scattering from mechanically exfoliated 2D MoO₃ nanolayers *2D Mater.* **2** 035004
- [57] Baibarac M, Smaranda I, Scocioreanu M, Mitran R A, Enculescu M, Galatanu M and Baltog I 2015 Exciton-phonon interaction in PbI₂ revealed by Raman and photoluminescence studies using excitation light overlapping the fundamental absorption edge *Mater. Res. Bull.* **70** 762–72
- [58] Wang Z, Zervas M N, Bartlett P N and Wilkinson J S 2016 Surface and waveguide collection of Raman emission in waveguide-enhanced Raman spectroscopy *Opt. Lett.* **41** 4146–9
- [59] Zhang T T, Wang C, Chen H, Zhang C Y, Zhang Z L, Fang Y R and Zheng H R 2019 Controlled multichannel surface plasmon polaritons transmission on atomic smooth silver triangular waveguide *Adv. Opt. Mater.* **7** 1900930
- [60] Wang Z 2016 *Waveguide enhanced raman spectroscopy (WERS): principles, performance, and applications* University of Southampton Doctoral dissertation
- [61] Mi Y et al 2019 High-quality hexagonal nonlayered CdS nanoplatelets for low-threshold whispering-gallery-mode lasing *Small* **15** e1901364
- [62] Mohammed S I, Al-Douri Y, Hashim U, Ahmed N M and Al-Gaashani R 2013 Structural and optical properties of PbI₂ nanostructures obtained using the thermal evaporation method *Can. J. Phys.* **91** 826–32